Upper limb compliant strategy exploiting external physical constraints for humanoid fall avoidance

Enrico Mingo Hoffman, Nicolas Perrin, Nikos G. Tsagarakis and Darwin G. Caldwell

Department of Advanced Robotics
Istituto Italiano di Tecnologia (IIT)
Via Morego 30, 1616 Genova

***Abstract*— Ensuring humanoid balance stability to prevent falling is one of the most crucial control problems in humanoid robotics and has been extensively studied in the past, resulting in a diverse range of balance recovery schemes. These balancing control methods effectively perform body posture control using three main motion strategies, namely: ankle, ankle-hip and stepping strategies. In this work we present a novel balance strategy which fundamentally differs from the previous methods as its principle is to exploit contacts with the environment to prevent falling rather than only performing body posture control. An uncoupled impedance controller for the upper body of the humanoid robot is combined with a lower body stabilizer, and the balancing capabilities are enhanced by the establishment of additional physical contacts with the environment. The generation of the reactive arm motion and the impedance regulation are discussed in details. Experimental trials with the humanoid robot COMAN, provided with active and passive compliance, demonstrate the potential of the approach and the first step towards the development of more human-like balancing skills using an integrated approach where all body parts (not only legs but also arms and hands) can establish contacts with the surrounding environment so as to ensure a stable and balanced behavior.**

I. Introduction

In the past fifteen years, the research on humanoid robots has gained huge attention by the robotics community. Several robotics challenges, such as the RoboCup or the recent DARPA Robotics Challenge, give researchers strong incentives to address problems specific to humanoid robot control such as balancing [1], walking [2], trajectory planning [3] and whole-body control [4]. Despite the progress made in all these areas there are still significant barriers to overcome before the control and motion performance of these machines enables them to operate outside the lab. Stable balancing, in planned and accidental physical interactions, is one of the fundamental skills in which humanoid robots currently underperform. This shortcoming is one of the key issues that makes it difficult for humanoid robots to operate in unstructured workspaces such as the ones designed for and used by humans.

In the existing literature of balancing control three main approaches can be identified, namely ankle [5], ankle-hip [6] and stepping strategies [7]. These methods can be applied in an individual or combined manner depending on the nature of the disturbance, and if the fall is inevitable, *safe fall* strategies have also been developed [8], [9].

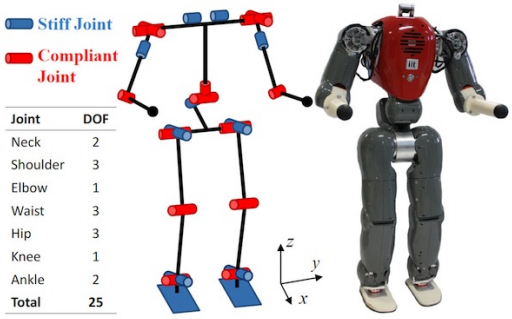

Fig. 1: A picture of the COmpliant huMANoid robot COMAN with its kinematic structure and DOFs.

The above balancing schemes are acting on the posture of the humanoid robot by controlling some important body state variables including but not limited to angular momentum, center of pressure and center of mass. Although these methods have demonstrated good balancing performance they lack a fundamental aspect of the human balancing skills as far as the use of the upper limbs is concerned. It can for example be observed that in humans, much of our balancing proficiency comes from our ability to use our body and arm motions to establish additional contacts with the environment and assist the locomotion and balancing in situations where simple body posture control or stepping actions are not adequate.

Inspired by this observation this work presents a novel balance strategy which fundamentally differs from previous methods as it exploits contacts with the environment using the arms to prevent falling rather than only performing body posture control. We believe that these upper limbs actions and the exploration of contacts with the environment can significantly extend the balancing performance of humanoids under severe disturbances, making them eventually capable of operating in realistic workspaces.

The proposed method combines two control strategies, one for the lower body and one for the upper body. The lower body runs an Inertial Measurement Unit (IMU) based balance controller that rejects small external disturbances and maintains the upper body upright posture during strong pushes. A second controller implemented on the upper body executes the arm motions necessary to establish contacts with the environment and support the balance of the robot. The initial configuration of the robot arms when the contacts with

the environment surface are established, is derived through an arm posture optimization that attempts to align the arm Cartesian stiffness ellipsoid with a desired orientation maximizing the compliance in the direction of the disturbance. Then, the impedance levels of the arms are dynamically regulated to improve the matching to the desired stiffness ellipsoid and to ensure that the reaction forces from the arm contacts are adequate to support the robot without inducing contact instabilities.

Impedance control has been widely applied on humanoid robots as an effective approach to ensure proper interactions and contact stability for a diverse range of tasks. For instance, in [10] an impedance control scheme for walking and balancing tasks was realized. Damping and stiffness parameters are modulated online to absorb impacts during the foot landing phase. [11] presents a whole-body control framework that uses impedance control laws and deals with physical limitations and collision avoidance, but results are demonstrated on a mobile-base humanoid robot. In [12], *Virtual Model Control*, an impedance control scheme for bipedal walking, is proposed and implemented on real robots. This method is based on the use of virtual components to obtain desired behaviors. For instance, it is shown that specifying desired forces for a virtual spring-damper placed between the foot and the waist can help to achieve walking on slopes or on uneven terrain with a planar bipedal robot.

In our approach, the triggering of the arm motion is based on the IMU measurements. The effectiveness of our strategy is demonstrated experimentally on the compliant humanoid COMAN (Fig. 1, [13]), which is able to sustain strong pushes by reaching a wall with its arms and then compliantly interacting with it. In the experiments the position of the wall is known with an accuracy of a few centimeters.

The presentation of the work is structured as follows: Section II presents the conceptual principle of our strategy, Section III briefly describes the lower body balance controller and presents in details the algorithms for the arms reactive motion and the impedance regulation. Finally in Section IV we discuss the experimental implementation and the results on the compliant humanoid robot COMAN while Section V addresses the conclusion.

II. Concept Principle

Let us consider the scenario shown in Fig. 2 with the robot standing in front of a physical wall. We assume that a basic stabilizer is running on the lower body with the aim of maintaining the upper body erect and slowing down its change of orientation. We correspondingly assume a *linear inverted pendulum* model for the robot. When the robot is pushed, the upper body moves on the transverse plane along the direction of the push. The motion of the arms is triggered when the waist of the robot exceeds the following threshold measured with the on-board IMU:

$$\theta_{th} = \arctan\left(\frac{L - x^*}{h}\right) \tag{1}$$

where x^* is the linear distance from the wall at which the arms motion should be triggered, and h is the height of the center of mass (CoM) considered constant.

Before the arm motion, an optimization is executed to derive the arm posture configuration and stiffness. The optimization problem takes into consideration the joint limits, the limit on the maximum achievable active joint stiffness and the constraint that the robot end-effectors must touch the wall. Once the robot end-effectors land on the wall, the arm joint stiffness is controlled actively. The joint damping is chosen proportional to the joint stiffness through a constant. The next section introduces the details of the proposed strategy.

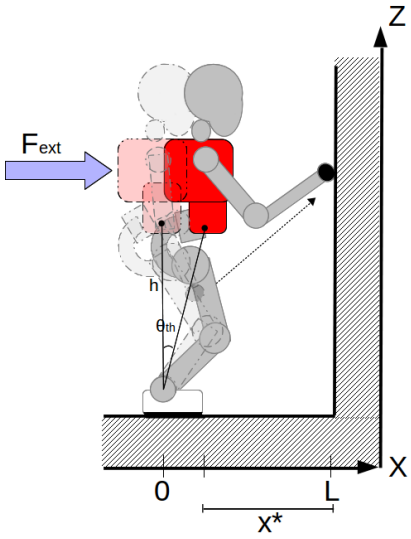

Fig. 2: The aim of our control scheme is to have the robot maintain its balance by using the wall as support.

III. Push Recovery Controller

A. Lower Body Stabilizer

Our lower body stabilizer uses as input the attitude information measured from the IMU mounted on the pelvis of the robot. Based on these measurements and on the proprioception, a closed-loop control law estimates the posture of the lower body in the world frame, and then modifies this posture through inverse kinematics so as to achieve the three main goals of keeping a horizontal motion of the center of mass, slowing down the attitude variations of the trunk, and acting as a low-pass filter that rejects high-frequency vibrations at the pelvis. These three properties of the lower body stabilizer do not prevent the robot from falling, but they lead to a smoother and more predictable motion of the robot trunk, even just after a push. Thanks to the effect of the stabilizer, it becomes a reliable choice to use a threshold on the trunk pitch whether the robot is about to fall or not, and thus whether the arms should start a motion to reach the wall or not. The algorithmic and mathematical description of this stabilizer is out of the scope of the present paper.

B. Arm Reaction Controller

The goal of the arm reaction controller is to generate the arm configuration and initial impedance values required to establish stable contacts with the environment and assist the robot recovery against a disturbance. To achieve this the arm controller generates the arm posture and joint stiffnesses so as to minimize the distance between a desired Cartesian stiffness ellipsoid and the one actually obtained.

The Cartesian stiffness of the robot arm is described by the stiffness matrix:

$$\mathbf{K}_C = -\frac{\partial \mathbf{f}}{\partial \mathbf{x}} \tag{2}$$

which represents the relation between the Cartesian wrench $\mathbf{f}$ and the Cartesian displacement $\mathbf{x}$. $\mathbf{K}_C \in R^{m\times m}$ where m is the number of Cartesian degrees of freedom. It is also possible to define a stiffness matrix in joint space as the relation between torques τ and displacement $\mathbf{q}$:

$$\mathbf{K}_q = -\frac{\partial \tau}{\partial \mathbf{q}} \tag{3}$$

$\mathbf{K}_q \in R^{n\times n}$ where n is the number of joints. From Maxwell's Reciprocal Theorem, all stiffness matrices are symmetric and in particular $\mathbf{K}_q$ is diagonal. The mapping from Cartesian stiffness $\mathbf{K}_C$ to joint stiffness $\mathbf{K}_q$ is given by:

$$\begin{aligned}\mathbf{K}_q &= -\frac{\partial \tau}{\partial \mathbf{q}} = -\frac{\partial (\mathbf{J}(\mathbf{q})^T \mathbf{K}_C \mathbf{J}(\mathbf{q})\Delta\mathbf{x})}{\partial \mathbf{q}} \\ &= \mathbf{J}(\mathbf{q})^T \mathbf{K}_C \mathbf{J}(\mathbf{q}) - \frac{\partial \mathbf{J}(\mathbf{q})}{\partial \mathbf{q}} \mathbf{K}_C \Delta\mathbf{x}\end{aligned} \tag{4}$$

where $\mathbf{J} = \frac{\partial \mathbf{T}(\mathbf{q})}{\partial \mathbf{q}}$ is the manipulator Jacobian, $\mathbf{T}(\mathbf{q})$ is the forward kinematic of the manipulator and $\Delta\mathbf{x} = \mathbf{x_d} - \mathbf{x}$ (see [14]) with $\mathbf{x_d}$ the equilibrium position. If the stiffness at equilibrium position is considered, then the second term in (4) disappears and it is reduced to:

$$\mathbf{K}_q = \mathbf{J}(\mathbf{q})^T \mathbf{K}_C \mathbf{J}(\mathbf{q}) \tag{5}$$

The inverse problem of (5) gives the Cartesian stiffness matrix:

$$\mathbf{K}_C = \mathbf{J}(\mathbf{q})^{\dagger T} \mathbf{K}_q \mathbf{J}(\mathbf{q})^{\dagger} \tag{6}$$

where $\mathbf{J}(\mathbf{q})^{\dagger} = {\mathbf{K_q}}^{-1}\mathbf{J}(\mathbf{q})^T(\mathbf{J}(\mathbf{q}){\mathbf{K_q}}^{-1}\mathbf{J}(\mathbf{q})^T)^{-1}$ is the pseudoinverse of $\mathbf{J}(\mathbf{q})$ (see [14]).

It is possible to formulate the inverse problem considering also the compliance matrices $\mathbf{C}_C$ and $\mathbf{C}_q$ defined as the inverses of the stiffness matrices:

$$\mathbf{C}_C = \mathbf{K}_C^{-1} \tag{7}$$

$$\mathbf{C}_q = \mathbf{K}_q^{-1} \tag{8}$$

Therefore based on the same reasoning made in (4) and (5) and considering (8):

$$\begin{aligned}\mathbf{C}_C &= \mathbf{J}(\mathbf{q})\mathbf{C}_q\mathbf{J}(\mathbf{q})^T \\ &= \mathbf{J}(\mathbf{q})\mathbf{K}_q^{-1}\mathbf{J}(\mathbf{q})^T\end{aligned} \tag{9}$$

Notice that in the Cartesian compliance matrix, no inverse Jacobian is needed, which makes the computation lighter, and that is why we use it in our approach.

Let us consider the case of a 2R planar manipulator where $\mathbf{q} = [q_1 \quad q_2]^T$ is the robot joint configuration and $\mathbf{K}_q = diag(k_{q1}, k_{q2})$ is the Joint stiffness matrix. In this case the translational Cartesian stiffness matrix and the joint stiffness matrix are both of size 2×2. For a given arm configuration the Cartesian stiffness ellipsoid has its major axis length and orientation along the eigenvector of the largest eigenvalue of $\mathbf{K}_C$ and the arctangent of the associated eigenvector. Let us now consider a desired ellipse characterized by λ_1, λ_2 and θ representing the major axis, minor axis and orientation angle of the major axis respectively. The associated desired Cartesian stiffness matrix $\mathbf{K}_{Cd}$ can be computed as:

$$\mathbf{K}_{Cd} = \mathbf{R}_z(\theta)\mathbf{S}_{\lambda_1,\lambda_2}\mathbf{R}_z(\theta)^{-1} \tag{10}$$

where $\mathbf{R}_z(\theta)$ is the rotation matrix about z of θ and $\mathbf{S}_{\lambda_1,\lambda_2}$ is the diagonal matrix of eigenvalues.

To derive the arm configuration we then setup an optimization problem that regulates the arm posture to match the orientation of the desired stiffness ellipse. Considering (7) and by multiplying both sides by $\mathbf{K}_C$:

$$\mathbf{C}_C\mathbf{K}_C = \mathbf{I} \tag{11}$$

leads in the following optimization problem:

$$\min_{\mathbf{q}} \|\mathbf{C}_C\mathbf{K}_{Cd} - \mathbf{I}\| \tag{12}$$

Since we want the arm end-effector to be placed on the wall, an equality constraint is added, which for instance in the XZ planar case of Fig. 2 has the form:

$$T_{x,ee}(\mathbf{q}) - \mu T_{z,ee}(\mathbf{q}) - \rho = 0 \tag{13}$$

where $\mathbf{T}_{p,ee} = [T_{x,ee} \quad T_{z,ee}]$ is the positional part of the forward kinematic $\mathbf{T}_{ee}$ of the end-effector and the wall is modelled in 2D as a line of equation $x = \mu z + \rho$. The resulting optimization problem is therefore:

$$\begin{aligned}&\min_{\mathbf{q}} \|\mathbf{C}_C\mathbf{K}_{Cd} - \mathbf{I}\| \\ s.t. \quad &T_{x,ee}(\mathbf{q}) - \mu T_{z,ee}(\mathbf{q}) - \rho = 0\end{aligned} \tag{14}$$

Additional inequality constraints are inserted to bound the joint position within certain limits:

$$\mathbf{q}_{min} \leq \mathbf{q} \leq \mathbf{q}_{max} \tag{15}$$

and to avoid the penetration of the arm in the wall:

$$T_{x,elbow}(q_1) - \mu T_{z,elbow}(q_1) - \rho \leq 0 \tag{16}$$

with $\mathbf{T}_{p,elbow}$ is the positional part of the forward kinematic $\mathbf{T}_{elbow}$ of the elbow.

Taking into account the passive joint elasticity presented in some of the joints of the compliant humanoid COMAN, the joint stiffness matrix was formulated by considering a series of two springs: a fixed passive k_{qf} and a variable active k_{qi} element (Fig.3) [15]. Thus, the elements k_{qj} of

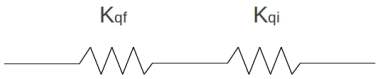

Fig. 3: Fixed Joint stiffness and variable Joint stiffness

$\mathbf{K}_q$ are computed as:

$$k_{qj} = \frac{k_{qfj} k_{qij}}{k_{qfj} + k_{qij}} \tag{17}$$

The achievable range of joint stiffness is added to the optimization problem as a set of linear inequality constraints that bound the joint active stiffness $\mathbf{K}_{qi} = [k_{qi1} \quad k_{qi2}]$ by $\mathbf{K}_{qimax}$:

$$\mathbf{0} \leq \mathbf{K}_{qi} \leq \mathbf{K}_{qimax} \tag{18}$$

Therefore, the optimization problem including the variable stiffness is:

$$\begin{aligned} \min_{\mathbf{q}, \mathbf{K}_{qi}} \quad & \|\mathbf{C}_C \mathbf{K}_{Cd} - \mathbf{I}\| \\ s.t. \quad & T_{x,ee}(\mathbf{q}) - \mu T_{z,ee}(\mathbf{q}) - \rho = 0 \\ & T_{x,elbow}(q_1) - \mu T_{z,elbow}(q_1) - \rho \leq 0 \\ & \mathbf{q}_{min} \leq \mathbf{q} \leq \mathbf{q}_{max} \\ & \mathbf{0} \leq \mathbf{K}_{qi} \leq \mathbf{K}_{qimax} \end{aligned} \tag{19}$$

This is a non-linear optimization problem in $\mathbf{q} = [q_1 \quad q_2]^T$ and $\mathbf{K}_{qi} = [k_{qi1} \quad k_{qi2}]$ with one non-linear equality constraint, two linear inequality constraints and one non-linear inequality constraint. The last one can be omitted if the distance from the robot to the wall is more than the length of the upper arm.

The optimization problem (19) tries to solve two tasks at the same time: an *inverse kinematics* task and the achievement of a desired Cartesian stiffness. Since, in our formulation, the position of the end-effector is treated as an equality constraint, this affects the achievable Cartesian stiffness as shown in Fig. 4.

In this work we consider a desired Cartesian stiffness ellipse with a large major axis parallel to the wall and a small minor axis so as to obtain a compliant behavior in the horizontal direction, but a stiff behavior if the end-effector is moving vertically to help the body to stay upright. Different ellipses can generate different behaviors and different arm postures, but we do not discuss in the present paper the possible choices for the desired Cartesian stiffness ellipse.

Furthermore, as explained in [14], the resulting optimization depends on the type and the weights of the norm used to calculate the optimization error. In our experiments we have chosen the *Weighted Frobenious Norm* [16], weighted with the desired Cartesian compliance. Finally, since (19) is a non-linear optimization problem, there is no algorithm that can ensure that the global optimum will be found in a reasonable time, and the final solution depends highly on the given initial guess. We explored a possible solution to this problem by using a *Particle Swarm Optimization* step to move towards a configuration that can be used as good initial guess for the optimization (19).

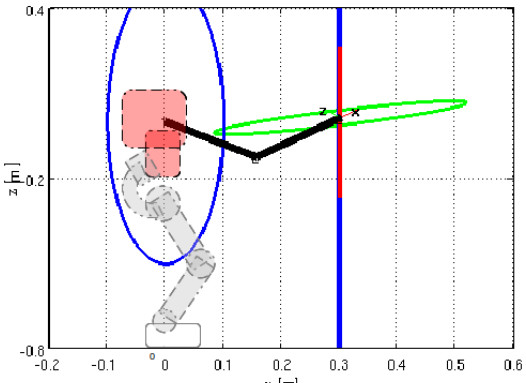

(a) A Cartesian stiffness ellipse parallel to the wall is difficult to achieve. $q_{fin} = [-0.67, 1.44]$, $\mathbf{K}_{qi} = diag(120.0, 120.0)$

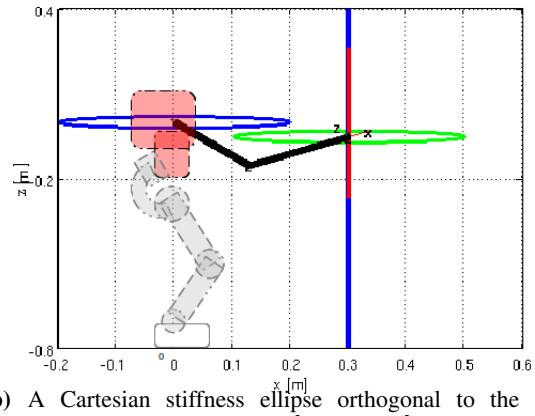

(b) A Cartesian stiffness ellipse orthogonal to the wall is achieved. $q_{fin} = [-0.87, 1.4]$, $\mathbf{K}_{qi} = diag(75.96, 96.68)$

Fig. 4: Examples of desired Cartesian stiffness (in blue) and obtained Cartesian stiffness (in green) ellipses.

C. Active Scaling of Stiffness Ellipse

Once the robot arms are in contact with the environment, forces such as its own body weight or external pushes act on it. A compliant behavior is necessary to sustain these external forces but at the same time the robot should not collapse.

In the case of our experiment, the optimized initial Cartesian stiffness ellipse obtained is far from the desired one (see Fig. 4). To obtain a behavior closer to the desired Cartesian stiffness ellipse, we use a simple algorithm that actively scales the actual Cartesian stiffness ellipse depending on the arm displacement (for example due to a push).

By multiplying all the joint stiffnesses by a scalar α, we can easily scale the Cartesian stiffness ellipse by the same coefficient α. $\mathbf{K}_C$ being the initial optimized Cartesian ellipse, when an arm end-effector moves by a displacement Δp, the problem we solve is the following:

$$\min_{\alpha} \|\alpha \mathbf{K}_C \Delta p - \mathbf{K}_{Cd} \Delta p\| \tag{20}$$

Equation (20) represents the equality of two force vectors, so it can be rewritten as:

$$\min_{\alpha} \|\alpha \mathbf{f}_C^* - \mathbf{f}_{Cd}\| \tag{21}$$

The solution is found by projecting $\mathbf{f}_{Cd}$ along $\mathbf{f}_C^*$ as shown in Fig. 5. We therefore obtain:

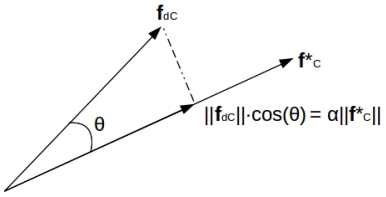

Fig. 5: Projection of $\mathbf{f}_{Cd}$ on $\mathbf{f}_C^*$.

$$\alpha = \frac{\|\mathbf{f}_{Cd}\|}{\|\mathbf{f}_C^*\|}\cos(\theta) \tag{22}$$

and $\cos(\theta)$ can be expressed as:

$$\cos(\theta) = \frac{f_{C,x}^* f_{Cd,x} + f_{C,z}^* f_{Cd,z}}{\|\mathbf{f}_C^*\|\,\|\mathbf{f}_{Cd}\|} \tag{23}$$

In our experiment, the initial total joint stiffnesses are all equal to $k_q = 60Nm/rad$, 50% of the value of the passive joint stiffnesses. To multiply these initial joint stiffnesses by α, we need to use the following formula (which considers the passive values) to set the variable stiffness values:

$$k_{qi} = \frac{\frac{\alpha}{2}}{1-\frac{\alpha}{2}} k_{qf} \tag{24}$$

We bound α between 1 and a minimum value ($\alpha_{min} < 1$). Fig. 7 shows the evolution of α as a function of Δx. We show the behavior of this control in Fig. 6.

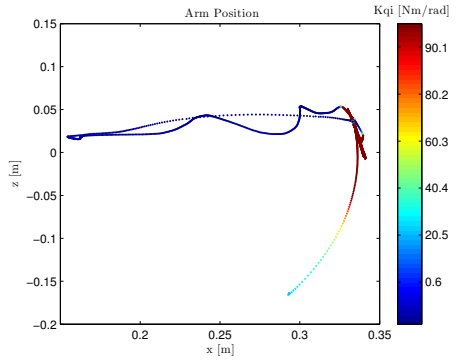

Fig. 6: Real data from COMAN left arm. Each point represents a pose $[x, z]$ for the end-effector. When the arm is stretched, vertical movements lead to actively controlled high set values of joint stiffnesses (in red) while the behavior becomes compliant when the arm is folded (in blue).

IV. Demonstration Test

We have tested our strategy on the compliant humanoid robot COMAN from the Italian Institute of Technology. The kinematic structure and the DOFs of COMAN are shown in Fig. 1. Since most of the joints are Series Elastic Actuated (SEA), COMAN is well suited for tasks that have to handle impacts.

The experiments are made with COMAN standing in front of the wall at a distance $L \simeq 0.3[m]$, and the arms' motion is triggered (i.e. the optimization) when the robot's horizontal

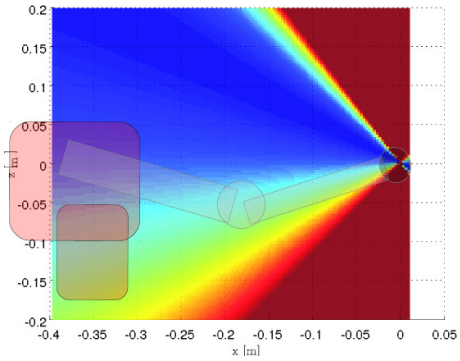

(a) α function, ZX view.

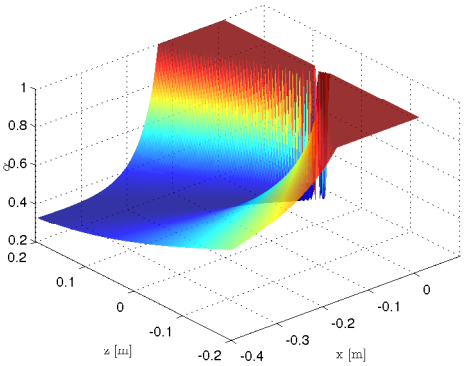

(b) α function, side view.

Fig. 7: α as a function of Δp.

motion exceeds a threshold of $x^* \simeq 0.15[m]$ corresponding to a $\theta_{th} = 0.3672[rad]$. The passive value of the joints stiffness is $\mathbf{K}_{qf} = diag(120.0, 120.0)[Nm/rad]$. Horizontal pushes are applied to the robot. The desired translational Cartesian stiffness matrix is:

$$\mathbf{K}_{Cd} = \begin{bmatrix} 0.2 & 0.0 \\ 0.0 & 1.0 \end{bmatrix} \cdot 1e^4[N/m]$$

The configuration obtained and resulting from the optimization is shown in Fig. 4a. The upper body of the COMAN is controlled using an impedance controller with an internal loop on the desired torques [17], while the waist and the lower body motions are controlled in position. The initial configuration of the robot upper body is set with low joint stiffnesses and as a result the arms stay down due to the gravity force. The stabilizer can easily handle small pushes but when the external force is large and the x^* threshold is exceeded, the optimization is performed, and the arms move towards the optimized configuration with the optimized joint stiffnesses. This behavior is shown in Fig. 8 from frames 1 to 6. Once COMAN is in contact with the wall, we continue to push it from both the shoulders at the same time. COMAN presents a compliant behavior when pushed and at the same time does not collapse on the obstacle. The single parameter α computed as explained in section III-C regulates the joint stiffnesses. This behavior of the robot is shown in Fig. 8 from frames 7 to 11.

To prove the robustness to different application points of

the external force, we push the robot only on one shoulder, and the pushes are well absorbed. This is shown in Fig. 8 from frames 12 to 16. The control scheme can handle variations in the distance to the wall and different configurations reached after the push w.r.t. to the one desired.

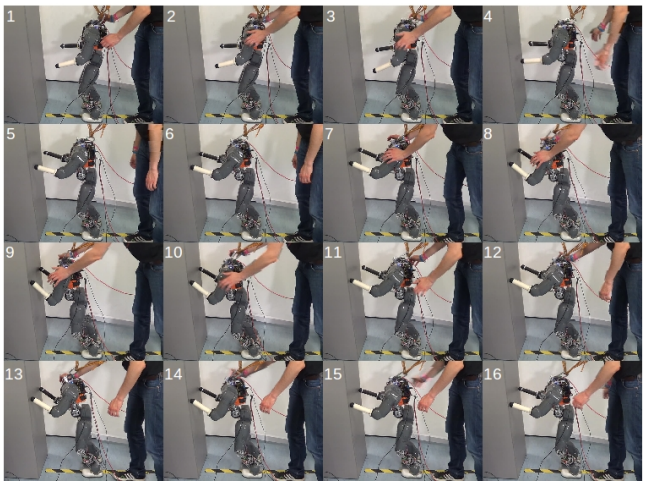

Fig. 8: Frames 1 to 6 show the reaction to a push. COMAN moves its arms towards the configuration computed from the optimization step. Frames 7 to 11 show the compliant behavior in case of an equally distributed push when COMAN is in contact with the environment. Frames 12 to 16 shows the same behavior in case of a non-equally distributed push.

V. Conclusion and Future Work

In this paper we have presented a novel, effective, model-free strategy to handle push recovery exploiting contacts with the environment for a humanoid robot. The main idea is based on the use of impedance control to handle the interaction between the arms and the environment. The lower body runs an IMU-based stabilizer algorithm to keep the balance, reject small disturbances and maintain the motion of the upper body on a plane. The upper body runs an impedance controller where joint configurations and stiffnesses are set based on a non-linear optimization achieved when the robot is going to fall due to a strong push. Once the robot is in contact with the environment, we actively vary the joint stiffnesses in order to be compliant to external horizontal perturbations. This results in a robust system that is able to lean over obstacles and recover from large pushes. This is a preliminary work for a framework that will handle omnidirectional disturbances and more complex environments. Two important aspects which are not discussed in this paper are: first, how to decide a desired translational Cartesian matrix, and second, how to vary the damping factor of the impedance controller. A reliable source of information regarding the arm stiffness during an impact can be taken from experiments with human subjects measuring the electrical activity of muscles through an electromyogram (EMG) [18]. A variable damping needs to depend on a dynamic model of the system taking into account external forces that need to be measured.

The integration with sensors that are able to recognize the local environment (for instance Kinect or cameras) will permit to design strategies to choose different surfaces where to place the arms. Finally, the possibility to merge this works with existing ones about stepping strategy, will lead to a more autonomous humanoid robot.

Ackowledgement

This work is supported by the FP7-ICT-2013-10 WALK-MAN European Commission project.

References

[1] B. Stephens, "Integral control of humanoid balance," in *in Proceedings of the IEEE/RSJ 2007 International Conference on Intelligent Robots and Systems*, 2007.

[2] S. Kajita, F. Kanehiro, K. Kaneko, K. Fujiwara, and K. H. K. Yokoi, "Biped walking pattern generation by using preview control of zero-moment point," in *in Proceedings of the IEEE International Conference on Robotics and Automation*, 2003, pp. 1620–1626.

[3] J. E. Chestnutt, M. Lau, G. K. M. Cheung, J. Kuffner, J. K. Hodgins, and T. Kanade, "Footstep planning for the honda asimo humanoid." in *ICRA*. IEEE, 2005, pp. 629–634.

[4] L. Sentis, J. Park, and K. Oussama, "Compliant control of multicontact and center-of-mass behaviors in humanoid robots." *IEEE Transactions on Robotics*, vol. 26, no. 3, pp. 483–501, June 2010.

[5] Z. Li, N. Tsagarakis, and D. G. Caldwell, "A passivity based admittance control for stabilizing the compliant humanoid coman," in *IEEE-RAS International Conference on Humanoid Robots*, Osaka, Japan, 2012.

[6] C. Ott, M. A. Roa, and G. Hirzinger, "Posture and balance control for biped robots based on contact force optimization." in *Humanoids*. IEEE, 2011, pp. 26–33.

[7] J. E. Pratt, J. Carff, S. V. Drakunov, and A. Goswami, "Capture point: A step toward humanoid push recovery." in *Humanoids*. IEEE, 2006, pp. 200–207.

[8] K. Fujiwara, F. Kanehiro, S. Kajita, K. Yokoi, H. Saito, K. Harada, K. Kaneko, and H. Hirukawa, "The first human-size humanoid that can fall over safely and stand-up again." *IROS*, pp. 1920–1926, October 2003.

[9] S.-K. Yun, A. Goswami, and Y. Sakagami, "Safe fall: Humanoid robot fall direction change through intelligent stepping and inertia shaping." *ICRA*, pp. 781–787, 2009.

[10] H.-o. Lim, S. A. Setiawan, and A. Takanishi, "Balance and impedance control for biped humanoid robot locomotion." in *International Conference on Intelligent Robots System*, vol. 1, November 2001, pp. 494–499.

[11] A. Dietrich, T. Wimböck, and A. Albu-Schäffer, "Dynamic whole-body mobile manipulation with a torque controlled humanoid robot via impedance control laws." in *IROS*. IEEE, 2011, pp. 3199–3206.

[12] J. E. Pratt, C.-M. Chew, A. Torres, P. Dilworth, and G. A. Pratt, "Virtual model control: An intuitive approach for bipedal locomotion." *I. J. Robotic Res.*, vol. 20, no. 2, pp. 129–143, 2001.

[13] N. G. Tsagarakis, G. M. Cerda, Z. Li, and D. G. Caldwell, "Compliant humanoid coman: Optimal joint stiffness tuning for modal frequency control." in *ICRA*, 2013, pp. 665–670.

[14] A. Albu-Schäffer, M. Fischer, G. Schreiber, F. Schoeppe, and G. Hirzinger, "Soft robotics: what cartesian stiffness can obtain with passively compliant, uncoupled joints?" in *IROS*. IEEE, 2004, pp. 3295–3301.

[15] T. Wimböck, C. Ott, A. Albu-Schäffer, A. Kugi, and G. Hirzinger, "Impedance control for variable stiffness mechanisms with nonlinear joint coupling." in *IROS*, 2008, pp. 3796–3803.

[16] Y. Wang, J. Lee, and Z. Jun, "Frobenius norm minimization and probing for preconditioning." *Int. J. Comput. Math.*, vol. 84, no. 8, pp. 1211–1223, 2007.

[17] M. Mosadeghzad, G. A. Medrano-Cerda, J. A. Saglia, N. G. Tsagarakis, and D. G. Caldwell, "Comparison of various active impedance control approaches, modeling, implementation, passivity, stability and trade-offs." pp. 342–348, 2012.

[18] A. Ajoudani, M. Gabiccini, N. G. Tsagarakis, A. Albu-Schaeffer, and A. Bicchi, "Tele-impedance: Exploring the role of common-mode and configuration-dependant stiffness." in *IEEE-RAS International Conference on Humanoid Robots*, Osaka, Japan, 2012, pp. 363–369.

ERRATUM

Section III, Subsection C:
"To multiply these initial joint stiffnesses by α,..." has to be changed to: "To multiply these initial joint stiffnesses by $\frac{\alpha}{2}$,...". This is needed because the admissible variable joint stiffness is bounded (in our case to a maximum of k_{qf}). In this way, when $\alpha = 1$ then $k_{qi} = k_{qf}$.

Section III, Subsection B:
Eq. [4] has to be corrected in:

$$\begin{aligned} \mathbf{K}_q &= -\frac{\partial \tau}{\partial \mathbf{q}} = -\frac{\partial (\mathbf{J}(\mathbf{q})^T \mathbf{K}_C \Delta \mathbf{x})}{\partial \mathbf{q}} \\ &= \mathbf{J}(\mathbf{q})^T \mathbf{K}_C \mathbf{J}(\mathbf{q}) - \frac{\partial \mathbf{J}(\mathbf{q})}{\partial \mathbf{q}} \mathbf{K}_C \Delta \mathbf{x} \end{aligned} \tag{25}$$